Title

Chlorophyll-carotenoid excitation energy transfer and charge transfer in *Nannochloropsis oceanica* for the regulation of photosynthesis.

Journal

Proceedings of the National Academy of Sciences of the United States of America, 116(9)

ISSN

0027-8424

Authors

Park, Soomin
Steen, Collin J
Lyska, Dagmar
et al.

Publication Date

2019-02-01

DOI

10.1073/pnas.1819011116

Peer reviewed

Chlorophyll–carotenoid excitation energy transfer and charge transfer in *Nannochloropsis oceanica* for the regulation of photosynthesis

Soomin Park[a,b,c,1], Collin J. Steen[a,b,c,1], Dagmar Lyska[b,d,1], Alexandra L. Fischer[a,b,c], Benjamin Endelman[b,d,e], Masakazu Iwai[b,d,e], Krishna K. Niyogi[b,d,e], and Graham R. Fleming[a,b,c,2]

[a]Department of Chemistry, University of California, Berkeley, CA 94720; [b]Molecular Biophysics and Integrated Bioimaging Division, Lawrence Berkeley National Laboratory, Berkeley, CA 94720; [c]Kavli Energy Nanoscience Institute, Berkeley, CA 94720; [d]Department of Plant and Microbial Biology, University of California, Berkeley, CA 94720; and [e]Howard Hughes Medical Institute, University of California, Berkeley, CA 94720

Contributed by Graham R. Fleming, December 17, 2018 (sent for review November 7, 2018; reviewed by Robert E. Blankenship and Barbara Demmig-Adams)

Nonphotochemical quenching (NPQ) is a proxy for photoprotective thermal dissipation processes that regulate photosynthetic light harvesting. The identification of NPQ mechanisms and their molecular or physiological triggering factors under in vivo conditions is a matter of controversy. Here, to investigate chlorophyll (Chl)–zeaxanthin (Zea) excitation energy transfer (EET) and charge transfer (CT) as possible NPQ mechanisms, we performed transient absorption (TA) spectroscopy on live cells of the microalga *Nannochloropsis oceanica*. We obtained evidence for the operation of both EET and CT quenching by observing spectral features associated with the Zea S_1 and $Zea^{\bullet+}$ excited-state absorption (ESA) signals, respectively, after Chl excitation. Knockout mutants for genes encoding either violaxanthin de-epoxidase or LHCX1 proteins exhibited strongly inhibited NPQ capabilities and lacked detectable Zea S_1 and $Zea^{\bullet+}$ ESA signals in vivo, which strongly suggests that the accumulation of Zea and active LHCX1 is essential for both EET and CT quenching in *N. oceanica*.

photosynthesis | nonphotochemical quenching | *Nannochloropsis* | charge transfer | excitation energy transfer

Photosynthetic organisms must balance the needs for efficient light harvesting and photoprotection depending on environmental conditions. As such, they have evolved important regulatory processes [frequently assessed from nonphotochemical quenching (NPQ)] that allow for the harmless dissipation of excessively excited chlorophyll (Chl*) during periods of high-light exposure, thereby minimizing the formation of reactive oxygen species and avoiding photooxidative stress (1, 2). Energy-dependent quenching (qE) is the fastest component of NPQ, becoming active on a timescale of a few seconds to minutes after high-light exposure (2). Due to its rapid response to light, qE plays a central role in photosynthetic organisms' ability to cope with fluctuating light conditions. Recent studies have shown that genetic manipulation of qE-related proteins in higher plants and green algae could be a promising way to increase biomass productivity and water use efficiency (3–5).

Extensive studies have aimed to uncover the molecular mechanisms involved in qE. The majority of these investigations utilize measurements of Chl fluorescence yield quenching, which are unable to provide information about the identity of the quenching species (6–8). Ultrafast transient absorption (TA) spectroscopy enables the detection of key species (e.g., carotenoid excited states) associated with specific mechanisms and can provide insight into the operation and timescales of the associated quenching. However, most TA experiments have used light-harvesting complex II (LHCII) or photosystem II (PSII) supercomplexes isolated from intact systems (9–15). Under in vivo conditions, transmembrane proton gradients (ΔpH), along with various interactions between pigment–protein complexes, control the induction and relaxation of qE (16, 17). Rapid relaxation of such gradients (18) and subtle changes in pigment–pigment and pigment–protein orientations and distances can alter the operation of qE-related processes (19–21). This suggests that observations from isolated proteins may not capture a full picture of the behavior of natural systems. Unfortunately, strong scattering makes fully intact systems (e.g., leaves, live cells) difficult to study using TA. However, isolated crude thylakoid membranes, which exhibit moderate quenching capabilities and less scattering, have been a useful sample for studying NPQ in the near-native state (22, 23). Nevertheless, there are significant differences between thylakoid membranes and fully intact systems in terms of the kinetics of qE induction/relaxation and the overall extent of quenching. These differences stem from regulatory loops, including feedback from the plant's sugar-consuming sink tissues. This makes it highly desirable to observe the operation of qE mechanisms in the fully native state.

The heterokont alga *Nannochloropsis oceanica* is a promising candidate for live-cell TA spectroscopy due to its small size (2–3 μm compared with ∼10 μm for the reference green alga *Chlamydomonas reinhardtii*) and high quenching capacity (NPQ ≅ 6). Recently, *N. oceanica* has attracted growing scientific and industrial interest due to its ability to accumulate high levels of polyunsaturated fatty acids and its high growth rate (24–26). Unlike land plants and green algae, its LHCs bind only Chl *a* and the carotenoids violaxanthin, antheraxanthin, and zeaxanthin (Vio–Anth–Zea) and vaucheriaxanthin (27, 28). This relatively simple pigment composition allows us to study qE mechanisms in a less complex system. *N. oceanica* also lacks the photosystem II subunit S

Significance

Manipulating the nonphotochemical quenching (NPQ) capabilities of photosynthetic organisms is known to result in increased crop productivity. However, optimization of yields also requires a detailed molecular understanding of the mechanism of NPQ in vivo with specific attention to the roles of the carotenoid zeaxanthin and various ΔpH-sensing proteins, such as photosystem II subunit S and stress-related antenna proteins (e.g., LHCX). Here, to investigate such in vivo NPQ mechanisms, we report transient absorption spectroscopy measurements on live cells of *Nannochloropsis oceanica*. We show that two fundamental processes proposed as NPQ mechanisms are active in *N. oceanica* and specifically require violaxanthin de-epoxidase as well as the LHCX1 protein. These findings have implications for optimizing the yields of algal biofuels.

Author contributions: S.P., C.J.S., D.L., A.L.F., K.K.N., and G.R.F. designed research; S.P., C.J.S., D.L., A.L.F., B.E., and M.I. performed research; S.P., C.J.S., A.L.F., and G.R.F. analyzed data; and S.P., C.J.S., D.L., K.K.N., and G.R.F. wrote the paper.

Reviewers: R.E.B., Washington University in St. Louis; and B.D.-A., University of Colorado.

Conflict of interest statement: K.K.N. and R.E.B. are coauthors on a 2015 Perspective article.

[1]S.P., C.J.S., and D.L. contributed equally to this work.

[2]To whom correspondence should be addressed. Email: grfleming@lbl.gov.

Published online February 11, 2019.

(PsbS) protein (29), which is necessary for qE in plants (30), but it has LHCX proteins (6, 31, 32) that are homologs of the stress-related LHCSR proteins that function in qE in green algae (33), mosses (34), and diatoms (35). *N. oceanica* also has a plant-type violaxanthin de-epoxidase (VDE) (29), which is a thylakoid lumen protein responsible for the accumulation of Zea in response to lumen acidification under high-light conditions. Although both LHCX1 and VDE are hypothesized to be NPQ components in *Nannochloropsis* species (6), it is still unclear which qE mechanisms are controlled by these two proteins under in vivo conditions.

Although the mechanisms of NPQ in *N. oceanica* remain to be determined, it is well known that electronic interactions between carotenoids (Car) and Chl play a major role in NPQ, and that coupled Chl–Car pairs can provide quenching sites (36–38). As shown in Scheme 1, two possible mechanisms of Chl–Car energy transfer and subsequent de-excitation have been reported to explain the role of Car as a direct quencher (23, 39). In the first, excitation energy transfer (EET) quenching can be achieved by energy transfer from the Chl Q_y state to the Car S_1 state (9, 10, 23, 40). Excitation energy that reaches a coupled Chl–Car pair undergoes rapid de-excitation because the lifetime of the Car S_1 state is much shorter (~10 ps) than that of Chl Q_y (>1 ns). Bidirectional energy transfer, Chl $Q_y \leftrightarrow$ Car S_1, has also been proposed under the condition that strong electronic coupling exists between the two states (41–43). Another possible mechanism, charge transfer (CT) quenching, involves the transient formation of a CT state composed of $Car^{\bullet+}$ and $Chl^{\bullet-}$ (12–15, 22, 44, 45). The excitation energy in the CT state is then de-excited through a charge recombination process (≥40 ps), followed by relaxation to the ground states. Ultrafast TA spectroscopy of plant thylakoid membranes has demonstrated that both the Car S_1 and $Car^{\bullet+}$ excited states are transiently populated following an initial Chl excitation, providing evidence for active EET and CT mechanisms, respectively (22, 23, 40, 45).

Here, to obtain insight into the possible roles of EET and CT mechanisms in the qE of *N. oceanica*, we performed live-cell TA spectroscopy in conjunction with Chl fluorescence lifetime snapshots and time-resolved HPLC measurements. We utilized *lhcx1* and *vde* mutants of *N. oceanica* that lack LHCX1 and VDE, respectively, to specifically investigate the involvement of these proteins. We show that both EET and CT mechanisms are active in wild type and that LHCX1 and VDE are essential for both mechanisms in *N. oceanica*.

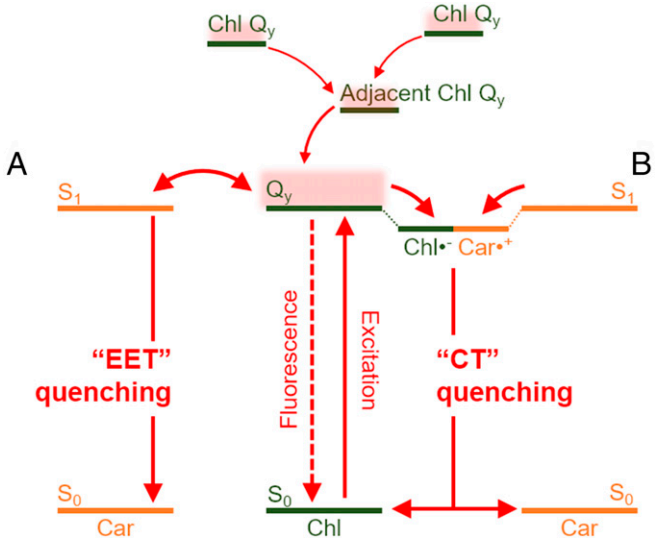

Scheme 1. Schematic illustration for the Chl–Car EET (*A*) and Chl–Car CT (*B*) quenching processes.

Results

Fig. 1 *A* and *B* shows the results of Chl fluorescence lifetime snapshots of *N. oceanica* live cells. The data are presented as amplitude-weighted average lifetime ($\tau_{average}$) and NPQτ values, respectively (calculations of $\tau_{average}$ and NPQτ are provided in *Materials and Methods*) (22, 23). The Chl fluorescence lifetime of wild-type *N. oceanica* decreased substantially from 1.25 to 0.22 ns during 10 min of high-light exposure (Fig. 1*A*), which is equivalent to an NPQτ value of 6.2. However, the *vde* and *lhcx1* mutants showed very low quenching (NPQτ ≅ 0.4), which was not rapidly reversible. It is apparent that active VDE and LHCX1 proteins in *N. oceanica* are necessary for qE induction.

Fig. 1*C* presents time-resolved HPLC data for the concentration of the Zea pigment in response to dark/light exposure. The data confirm that the *vde* mutant lacks the ability to accumulate Zea due to the absence of the VDE enzyme. In contrast, wild type and the *lhcx1* mutant actively accumulate Zea in response to high-light exposure, although the accumulation of Zea in the *lhcx1* mutant was lower than in the wild type. The reverse reaction of epoxidation (Zea → Anth → Vio) during the dark recovery period was clearly slower than that of de-epoxidation. Given that the NPQτ value of the wild type was significantly lowered (6.2 → 0.8) following dark recovery despite only a small change in Zea concentration (−8.7%), the level of NPQ was not strictly correlated with the concentration of Zea. These observations suggest the existence of other qE feedback processes beyond the Vio–Anth–Zea cycle, such as sensing of the transthylakoid ΔpH, in which the LHCX1 protein is presumably involved.

To investigate the activation of the EET mechanism upon high-light exposure, we measured the Zea S_1 excited-state absorption (ESA) signal in *N. oceanica* cells before and after high-light exposure (Fig. 2*A*). As shown in Scheme 1*A*, an active EET quenching pathway results in transient population of the Zea S_1 state after Chl *a* excitation (665 nm), which can be probed at 540 nm (Zea S_1–S_N transition) (23, 40). Because a significant amount of Chl *a* ESA signal is also detected at this wavelength, the signals measured at 540 nm after high-light exposure are a combination of Zea S_1 ESA and Chl ESA. Because high light activates a variety of de-excitation pathways, the Chl excited-state population should be lower in high-light–exposed cells, and, indeed, the amplitude of the Chl ESA significantly decreases. This accounts for the overall lower amplitude of the ESA signal at 540 nm after high-light exposure despite the rapid contribution of the Zea S_1 ESA at early time delays (Fig. 2*A*). When we compared the kinetics of the ESA signals measured in the dark and in high light, the two profiles were kinetically equivalent at time delays ≥40 ps. This ESA signal at longer time delays can mainly be attributed to the Chl ESA since the Zea S_1 states are almost entirely de-populated by this time delay. We therefore scaled the kinetic profile measured in the dark (mostly Chl ESA) to match that in high light based on signals at about 40 ps. Subtraction of the scaled dark signal from the high-light signal allows us to extract the contribution of Zea S_1 ESA from the overall Chl ESA. The Zea S_1 ESA profiles (Fig. 2*B*) showed a single exponential decay with a lifetime of 7.71 ps and no resolvable rise time within the time resolution (~120 fs) of our TA setup. The lifetime of this difference signal coincides with literature values for the S_1 lifetime of Zea, which range from 7 to 11 ps (23, 40, 46, 47). Additionally, the difference spectrum (Fig. 2*A*, *Inset*) clearly resembles the Car S_1 ESA spectrum observed in both methanol (47) and isolated thylakoid membranes (23, 40). We considered whether the well-known transient electrochromic shift of the Car S_0–S_2 absorption resulting from the light-induced transmembrane electric field (ΔΨ) could give rise to the signal at 540 nm. Typical electrochromic shift spectra show peaks between 515 and 520 nm in various plants and green algae (48), while the difference spectrum (Fig. 2*A*, *Inset*) has peak absorption at 540 nm and no absorption at 520 nm. This, along with the lifetime of this feature, suggests

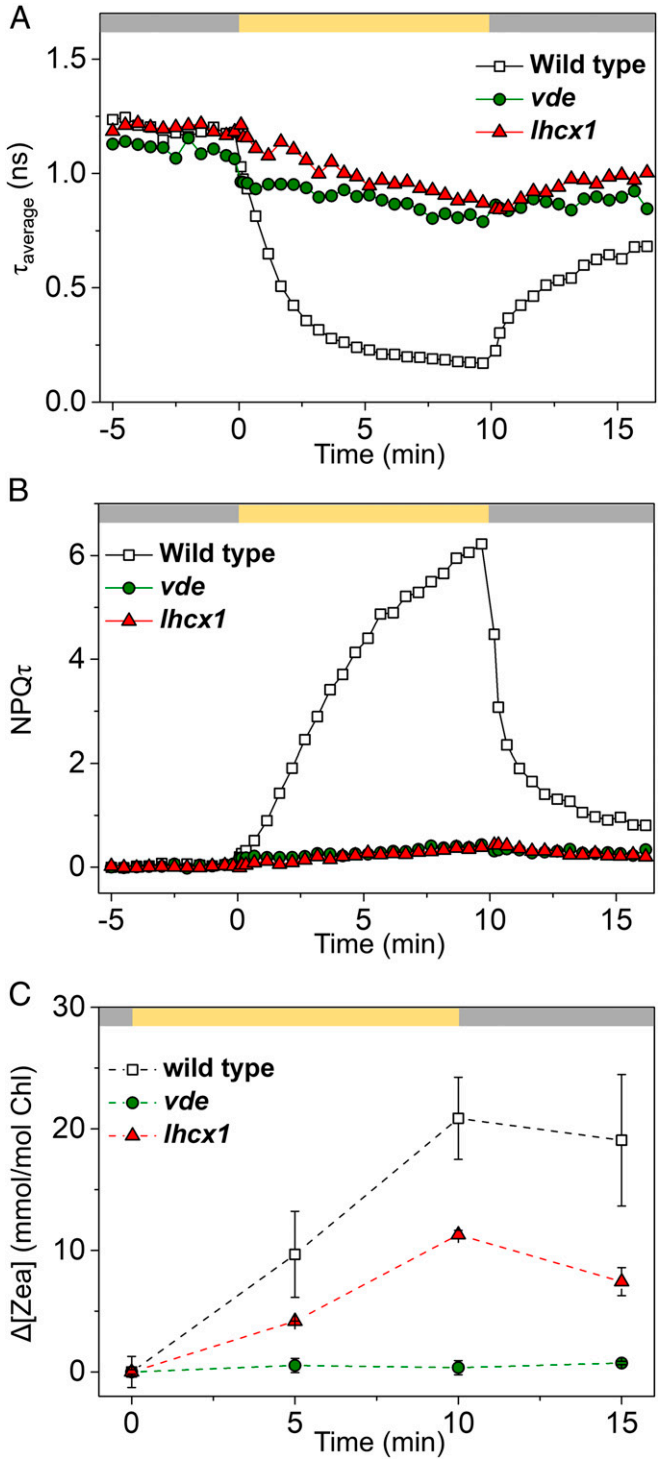

Fig. 1. Fluorescence lifetime snapshot results presented as average Chl fluorescence lifetime ($\tau_{average}$) (*A*) and calculated NPQτ values for wild type (white squares), *vde* mutant (green circles), and *lhcx1* mutant (red triangles) (*B*) in response to dark/high-light exposure. Bars at the top of the figures indicate the time sequence of actinic light on (yellow, 850 μmol of photons per $m^{-2}{\cdot}s^{-1}$) and off (dark gray). A detailed discussion of $\tau_{average}$ and calculated NPQτ values is provided in *Materials and Methods*. (*C*) Kinetics of Zea concentration determined by time-resolved HPLC measurements. Data are presented as the mean ± SD ($n = 3$).

that the difference signal most likely comes from Car S_1–S_N absorption. The lack of positive difference signals from *vde* and *lhcx1* mutants (Fig. 3 *A* and *C*) further supports this conclusion.

Chl*–Chl* annihilation is present at the intensities necessary for our TA measurements. This additional loss mechanism for excited Chl results in a decrease of the excitation diffusion length. The presence of annihilation is signaled by the decrease in the Chl fluorescence lifetime, which ranged from 0.22 to 1.25 ns (Fig. 1*A*) under annihilation-free conditions, significantly longer than the Chl ESA signal lifetime ($\tau_{average} \leq 0.1$ ns) observed in our TA measurement (Fig. 2*A*). In this condition, the Chl*–Chl* annihilation dominantly affects the Chl ESA decay kinetics. Given that the annihilation rate is constant during the transition from dark to high light, Chl ESA in dark and high light should have kinetically equivalent decays, which allows us to extract the Car S_1 ESA signal as the difference between dark and high-light TA profiles (23). In addition, the presence of significant annihilation suggests that only those Chls that are excited in close proximity to Car molecules will populate the Car S_1 state we observe via TA. In this regard, the key observation in our Zea S_1 ESA kinetic profile (Fig. 2*B*) is the lack of a resolvable rise time, which suggests near-instantaneous excitation energy equilibrium between the excited states of Zea and Chls nearby to Zea. The results of a kinetic simulation of the Zea S_1 state population with specific consideration of annihilation processes were described in our recent study (23).

Fig. 2*C* shows the ESA signals measured at 980 nm, where $Zea^{\bullet+}$ peak absorption appears (14, 22, 45) before and after high-light exposure of *N. oceanica* cells. Multiple species (e.g., ^{1}Chl*, ^{3}Chl*, ^{1}Car*) have ESA at 980 nm, making it difficult to deconvolute the individual species and corresponding ESA in the intact system. However, in the absence of $Zea^{\bullet+}$ ESA, we observed no noticeable change in the amplitude of the 980-nm ESA signal upon high-light exposure (Fig. 3), which is consistent with our previous observations in thylakoid membranes (22, 45). Therefore, the dark and high-light kinetic profiles in Fig. 2*C* do not need to be normalized in any way. The difference ESA signal between the high-light and dark conditions (Fig. 2*D*) corresponds to the kinetic profile of $Zea^{\bullet+}$ and exhibits both rise (0.61 ps) and decay (40 ps) components. Unlike the Zea S_1 ESA, the $Zea^{\bullet+}$ ESA profile has a resolvable rise component ($\tau_{rise} = 0.61$ ps). We believe this is due to the slower (~40 ps) charge recombination process for CT states ($Zea^{\bullet+}$–$Chl^{\bullet-}$), which allows excitation energy to be transferred to and populate the Chl–Zea pair before dissipation (23). Interestingly, the same $Zea^{\bullet+}$ decay time (40 ps) was observed from high-light–exposed spinach thylakoid membranes in our recent study (22). However, the rise time constant (0.61 ps) from *N. oceanica* was significantly smaller than that from spinach thylakoid membranes (15.4 ps) (22). This difference may be due to different antenna sizes and structures, which could influence the extent of annihilation and the kinetics of excitation transfer and trapping within PSII.

We took advantage of *lhcx1* and *vde* knockout mutants to investigate the specific roles of the LHCX1 and VDE proteins in the EET and CT mechanisms. In the *lhcx1* mutant, no noticeably positive ESA signal was observed (Fig. 3 *A* and *B*); thus, neither the Zea S_1 nor $Zea^{\bullet+}$ state appears to be present. This observation strongly suggests that the LHCX1 protein is necessary for activation of both EET and CT quenching. We were also unable to observe either Zea S_1 or $Zea^{\bullet+}$ ESA in the *vde* mutant (Fig. 3 *C* and *D*), indicating that accumulated Zea is also necessary for the EET and CT mechanisms in *N. oceanica*. In addition to lacking active EET and CT mechanisms, both the *lhcx1* and *vde* mutants exhibited negligible overall Chl* quenching in response to high-light exposure (Fig. 1 *A* and *B*), further supporting the idea that both EET quenching and CT quenching play a central role in Chl* de-excitation in high light.

Discussion

Our data clearly provide evidence that both Chl–Zea EET and CT mechanisms are active in intact live cells of *N. oceanica*. Our data do not specifically identify the quenching site(s) in *N. oceanica*, but the data in Figs. 1 and 3 strongly suggest that LHCX1 may be both the sensor of ΔpH and the actual site of

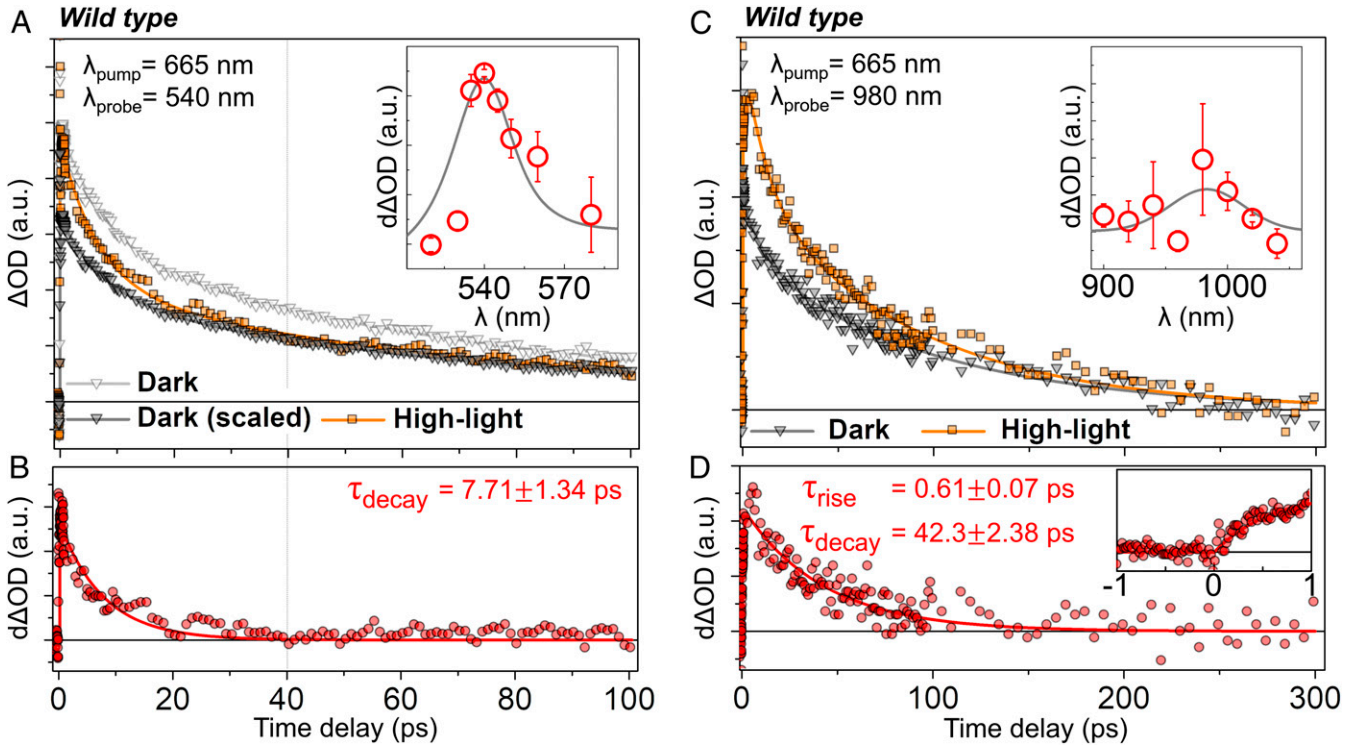

Fig. 2. TA kinetic profiles for *N. oceanica* cells after Chl *a* excitation at 665 nm. (*A*) Profiles for wild-type *N. oceanica* probed at 540 nm under dark (light gray, inverted triangles) and high-light (orange squares) conditions. The samples were exposed to an actinic light (850 μmol of photons per $m^{-2}{\cdot}s^{-1}$) for 15 min of high-light exposure. The scaled dark profile (dark gray, inverted triangles) is also displayed. (*Inset*) Graph shows the difference TA spectrum reconstructed by subtracting the scaled dark signal from the high-light signal at 1 ps. Each data point is presented as the mean ± SE ($n = 5$). The spectrum of the Car S_1 ESA (gray line) from spinach thylakoid membranes is also shown in the *Inset* as a reference (23). (*B*) Difference between high-light and scaled dark kinetic profiles measured at 540 nm. The lifetime obtained from fitting with a single exponential decay is 7.71 ± 1.34 ps. (*C*) Profiles probed at 980 nm under dark (dark gray, inverted triangles) and high-light (orange squares) conditions. These profiles are not normalized. (*Inset*) Graph shows the difference TA spectrum reconstructed by subtracting the dark signal from the high-light signal at 20 ps. Each data point is presented as the mean ± SE ($n = 5$). The gray curve represents the Gaussian fit to the difference data. (*D*) Difference between high-light and dark kinetic profiles measured at 980 nm. The lifetimes of the rise (τ_{rise}) and decay (τ_{decay}) components are 0.61 ± 0.07 ps and 42.3 ± 2.38 ps, respectively. ΔOD, changes in optical density; dΔOD, changes in ΔOD.

quenching. The finding that Zea accumulation alone produces little qE and no detectable Zea S_1 or $Zea^{\bullet+}$ makes it highly likely that Zea binding to LHCX1 is essential for qE in *N. oceanica*, and that Zea binding to other light-harvesting proteins does not produce significant qE under the conditions of our experiments. Given that the propensity for either Chl–Zea energy transfer or change transfer is very sensitive to the spatial separation of the pair (44), it is possible that a natural (or controlled) distribution of Chl–Zea separations and energy gaps within Zea–LHCX1* results in some quenching of excited Chl by EET and some by CT.

Both mechanisms require the VDE and LHCX1 proteins, which are activated by the formation of high-light–induced ΔpH across the thylakoid membrane (49) (Scheme 2). In this picture, Zea produced by VDE binds to LHCX1* to generate a Zea–LHCX1* pigment–protein complex similar to that observed in green algae and moss (12, 50). The quenching sites associated with this Zea–LHCX1* pigment complex are switched on and off by at least two in vivo control systems, one based on the concentration of Zea pigment and one based on activated LHCX1. An NPQ value (NPQτ) of 6 suggests that the Zea–LHCX1* combination is a remarkably effective quencher. If the model for green plant thylakoid membranes developed by Bennett et al. (51) applies to *N. oceanica*, an NPQ value of 6 implies an excitation diffusion length of less than 20 nm (figure 4 of ref. 51).

Conclusions

It has been shown that it is possible to improve crop yield by modification of the NPQ response through overexpression of three genes (3), one specifically encoding for the ΔpH-sensing protein (PsbS) and the other two encoding the enzymes responsible for interconversion between Zea and Vio via the xanthophyll cycle. To explore how large an increase in yield is possible, a mechanism for the role of Zea is needed. Measurements on isolated complexes lacking the full complexity of the intact system with its various feedback loops, sensing/activating proteins (e.g., PsbS or LHCSR/LHCX), and protein–protein interactions, along with pH and ionic gradients, do not capture the behavior of the in vivo system. Although subject to much speculation, no demonstration of the direct involvement of Zea in intact systems (e.g., live cells, leaves) had been made before this work. Specifically, the application of TA spectroscopy to live cells of *N. oceanica* enabled us to observe the operation of the Chl–Zea EET and CT mechanisms and their control systems in vivo. Building upon our previous observations from spinach thylakoid membranes, which showed that both the EET and CT mechanisms are involved in qE and are controlled by PsbS (22, 23), the present evidence further supports that the presence of de-epoxidized xanthophylls (e.g., Zea) and a ΔpH-sensing protein (e.g., LHCX, LHCSR, PsbS) is essential for the operation of both EET and CT mechanisms of qE in a variety of photosynthetic organisms. Developing a fundamental understanding of the qE mechanisms operating in vivo should provide a basis for increasing the yield of *N. oceanica*, which is a promising source for renewable biodiesel (24–26).

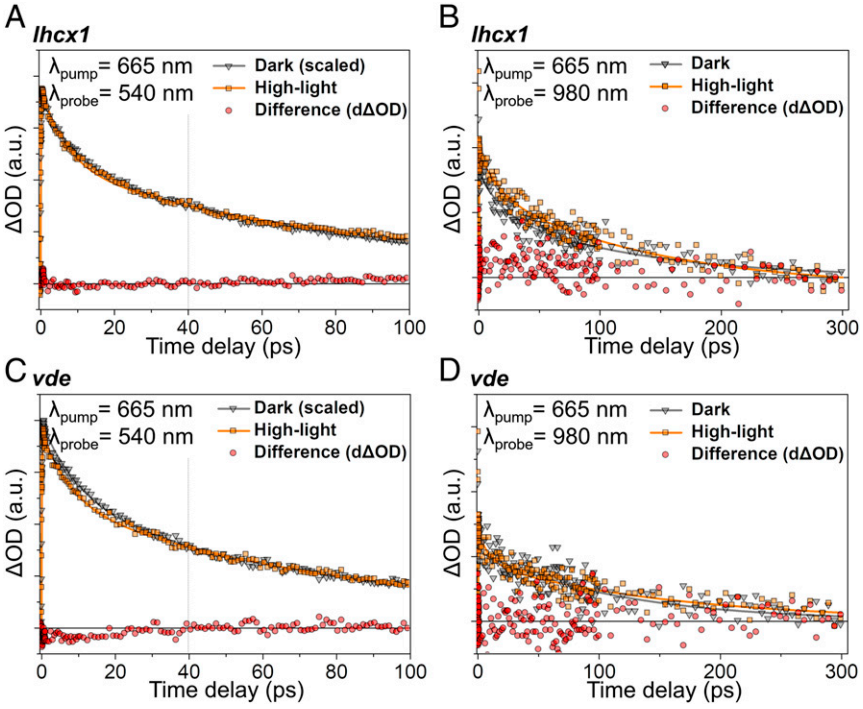

Fig. 3. TA kinetic profiles of *lhcx1* (*A*) and *vde* (*C*) mutants probed at 540 nm under dark (gray inverted triangles) and high-light (orange squares) conditions, as well as the difference (dΔOD, red circles) between high light and dark. The samples were exposed to an actinic light (850 μmol of photons per $m^{-2}{\cdot}s^{-1}$) for 15 min of high-light exposure. Note that the dark profiles in *A* and *C* are scaled to match the high-light profiles at 40 ps. Profiles of *lhcx1* (*B*) and *vde* (*D*) mutants probed at 980 nm under dark (gray inverted triangles) and high-light conditions (orange squares), as well as the difference (dΔOD, red circles) between high light and dark. The dark and high-light kinetic profiles in *B* and *D* were not normalized. ΔOD, changes in optical density.

Materials and Methods

Strains, Growth Conditions, and Sample Preparation. *N. oceanica* CCMP1779 wild type and *vde* and *lhcx1* mutant strains were grown in F2N medium under low-light conditions (30 μmol of photons per $m^{-2}{\cdot}s^{-1}$) until late-exponential phase (~5×10^7 cells per milliliter). The Chl *a* concentration was determined based on the calculation described by Porra et al. (52). The cell suspension for TA measurements was adjusted to 80 μg Chl *a* per milliliter by centrifuging the culture at 3220 × *g* for 5 min and resuspending the pellet in 20% (wt/vol) Ficoll in 20 mM Hepes-KOH (pH 7.2). The samples were dark-acclimated for 30 min and transferred to a cuvette for spectroscopic measurements.

TA Spectroscopy. The pump-probe TA spectroscopy setup was similar to those described in previous works by Park et al. (22, 23). Briefly, the pump beam, generated by optical parametric amplification of the 800-nm fundamental of an amplified Ti/sapphire laser at a repetition rate of 250 kHz, was centered at 665 nm for the Chl Q_y transition. The pump pulses had an energy of 40 nJ per pulse, and the FWHM of the autocorrelation trace was 42 fs. The probe beam was a white-light continuum, created by focusing the 800-nm laser on either a 1-mm-thick sapphire or 1-mm-thick yttrium aluminum garnet crystal, which exhibits greater conversion efficiencies in the visible and near-infrared (NIR) ranges, respectively. A 700-nm short-pass filter or 850-nm long-pass filter was placed after the crystal for visible and NIR continuum generation, respectively. The polarizations of the pump and probe were set to the magic angle (54.7°). The diameters of the pump and probe at the sample position were 140 μm and 65 μm, respectively. After the sample, a second polarization filter set to the probe polarization and a 658 ± 26-nm notch filter were placed to minimize pump scattering and ensure a clean probe signal. After a monochromator (SpectraPro 300i; Acton Research Corp.), Si (DET10A; Thorlabs), and InGaAs (DET410; Thorlabs) photodiodes were used to monitor the changes in absorption signal in the visible and NIR ranges, respectively. The cross-correlation between pump and probe was around 120 fs. The actinic light was set to an intensity of 850 μmol of photons per $m^{-2}{\cdot}s^{-1}$ at the sample position after a heat-absorbing filter (KG1). The sample solution was gently stirred between measurements, and the sample cuvette was translocated continuously during measurements to prevent sample damage. The path length of the cuvette was 1 mm.

Fluorescence Lifetime Snapshot. Our home-built fluorescence lifetime snapshot apparatus has been described in detail previously (22, 23, 53). The excitation laser power was 1.6 mW (21 pJ per pulse), and an actinic light (Schott KL1500) was set to an intensity of 850 μmol of photons per $m^{-2}{\cdot}s^{-1}$ at the sample. After fitting the fluorescence decays collected upon excitation at 680 nm with two exponential decay components, the $\tau_{average}$ (τ_{avg}) and NPQ_τ values were calculated by the following equations (22, 23, 54):

$$\tau_{avg} = \frac{\sum_i A_i \tau_i}{\sum_i A_i},$$

where A_i and τ_i are the amplitudes and the fluorescence lifetime components, respectively, and

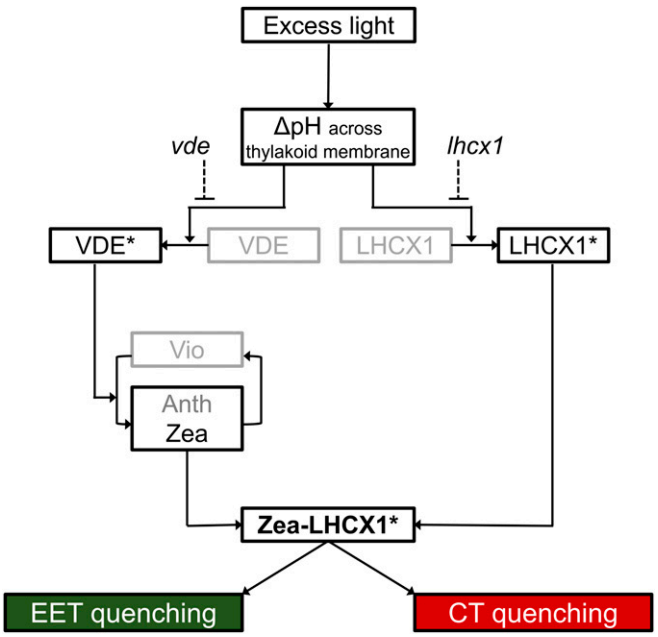

Scheme 2. Proposed scheme for the triggering system of the EET and CT quenching mechanisms for qE in *N. oceanica*. VDE* and LHCX1* indicate activated VDE and LHCX1 proteins, respectively. We hypothesize that Zea produced by VDE binds to LHCX1* to generate a pigment–protein complex that is necessary for both EET and CT quenching mechanisms.

$$\mathrm{NPQ} = \frac{\tau_{avg,dark} - \tau_{avg,light}}{\tau_{avg,light}},$$

where $\tau_{avg,dark}$ is the average of three lifetimes measured at the initial dark period.

HPLC Analysis of Pigments. Cells were prepared as described above. Five hundred microliters of the cell suspension was dark-acclimated in the cuvette for 30 min, followed by a 10-min light exposure (850 μmol of photons per $m^{-2}{\cdot}s^{-1}$) and a 5-min dark recovery phase. Aliquots of 100 μL for HPLC analysis were frozen in liquid nitrogen after dark acclimation, 5 and 10 min of illumination, and 5 min of dark recovery. For pigment extraction, the cells were thawed at room temperature and pelleted at 10,000 × *g* for 5 min. The supernatant was removed, and the pellet was frozen again in liquid nitrogen. Cells were broken (6.5 $m{\cdot}s^{-1}$ for 60 s) using the cryorotor of a Fastprep-24 (MP Bio) and extracted with 100 μL of acetone by vortexing. Cell debris was pelleted at 21,000 × *g* for 5 min. The pellet was extracted a second time with 100 μL of acetone, and the supernatants were pooled. Extracted pigments were analyzed with a Spherisorb 5-μm ODS1 column (Waters Corp) as described by Müller-Moulé et al. (55).

ACKNOWLEDGMENTS. G.R.F. thanks Magdalen College Oxford and the Department of Physical and Theoretical Chemistry at the University of Oxford for their hospitality while this paper was being written. This work was supported by the US Department of Energy, Office of Science, Basic Energy Sciences, Chemical Sciences, Geosciences, and Biosciences Division under Field Work Proposal 449B. K.K.N. is an investigator of the Howard Hughes Medical Institute.

1. Tripathy BC, Oelmüller R (2012) Reactive oxygen species generation and signaling in plants. *Plant Signal Behav* 7:1621–1633.
2. Müller P, Li X-P, Niyogi KK (2001) Non-photochemical quenching. A response to excess light energy. *Plant Physiol* 125:1558–1566.
3. Kromdijk J, et al. (2016) Improving photosynthesis and crop productivity by accelerating recovery from photoprotection. *Science* 354:857–861.
4. Głowacka K, et al. (2018) Photosystem II subunit S overexpression increases the efficiency of water use in a field-grown crop. *Nat Commun* 9:868.
5. Berteotti S, Ballottari M, Bassi R (2016) Increased biomass productivity in green algae by tuning non-photochemical quenching. *Sci Rep* 6:21339.
6. Chukhutsina VU, Fristedt R, Morosinotto T, Croce R (2017) Photoprotection strategies of the alga Nannochloropsis gaditana. *Biochim Biophys Acta Bioenerg* 1858:544–552.
7. Amarnath K, Zaks J, Park SD, Niyogi KK, Fleming GR (2012) Fluorescence lifetime snapshots reveal two rapidly reversible mechanisms of photoprotection in live cells of Chlamydomonas reinhardtii. *Proc Natl Acad Sci USA* 109:8405–8410.
8. Nilkens M, et al. (2010) Identification of a slowly inducible zeaxanthin-dependent component of non-photochemical quenching of chlorophyll fluorescence generated under steady-state conditions in Arabidopsis. *Biochim Biophys Acta* 1797:466–475.
9. Staleva H, et al. (2015) Mechanism of photoprotection in the cyanobacterial ancestor of plant antenna proteins. *Nat Chem Biol* 11:287–291.
10. Ruban AV, et al. (2007) Identification of a mechanism of photoprotective energy dissipation in higher plants. *Nature* 450:575–578.
11. Walla PJ, Linden PA, Ohta K, Fleming GR (2002) Excited-state kinetics of the carotenoid S1 state in LHC II and two-photon excitation spectra of lutein and β-carotene in solution: Efficient Car S1→Chl electronic energy transfer via hot S1 states? *J Phys Chem A* 106:1909–1916.
12. Bonente G, et al. (2011) Analysis of LhcSR3, a protein essential for feedback de-excitation in the green alga Chlamydomonas reinhardtii. *PLoS Biol* 9:e1000577.
13. Avenson TJ, et al. (2009) Lutein can act as a switchable charge transfer quencher in the CP26 light-harvesting complex. *J Biol Chem* 284:2830–2835.
14. Ahn TK, et al. (2008) Architecture of a charge-transfer state regulating light harvesting in a plant antenna protein. *Science* 320:794–797.
15. Avenson TJ, et al. (2008) Zeaxanthin radical cation formation in minor light-harvesting complexes of higher plant antenna. *J Biol Chem* 283:3550–3558.
16. Correa-Galvis V, Poschmann G, Melzer M, Stühler K, Jahns P (2016) PsbS interactions involved in the activation of energy dissipation in Arabidopsis. *Nat Plants* 2:15225.
17. Sacharz J, Giovagnetti V, Ungerer P, Mastroianni G, Ruban AV (2017) The xanthophyll cycle affects reversible interactions between PsbS and light-harvesting complex II to control non-photochemical quenching. *Nat Plants* 3:16225.
18. Zaks J, Amarnath K, Kramer DM, Niyogi KK, Fleming GR (2012) A kinetic model of rapidly reversible nonphotochemical quenching. *Proc Natl Acad Sci USA* 109: 15757–15762.
19. Balevičius V, Jr, et al. (2017) Fine control of chlorophyll-carotenoid interactions defines the functionality of light-harvesting proteins in plants. *Sci Rep* 7:13956.
20. Hontani Y, et al. (2018) Molecular origin of photoprotection in cyanobacteria probed by watermarked femtosecond stimulated Raman spectroscopy. *J Phys Chem Lett* 9:1788–1792.
21. Liguori N, et al. (2017) Different carotenoid conformations have distinct functions in light-harvesting regulation in plants. *Nat Commun* 8:1994.
22. Park S, et al. (2017) Snapshot transient absorption spectroscopy of carotenoid radical cations in high-light-acclimating thylakoid membranes. *J Phys Chem Lett* 8:5548–5554.
23. Park S, et al. (2018) Chlorophyll-carotenoid excitation energy transfer in high-light-exposed thylakoid membranes investigated by snapshot transient absorption spectroscopy. *J Am Chem Soc* 140:11965–11973.
24. Adarme-Vega TC, et al. (2012) Microalgal biofactories: A promising approach towards sustainable omega-3 fatty acid production. *Microb Cell Fact* 11:96.
25. Simionato D, et al. (2011) Acclimation of Nannochloropsis gaditana to different illumination regimes: Effects on lipids accumulation. *Bioresour Technol* 102:6026–6032.
26. Chisti Y (2007) Biodiesel from microalgae. *Biotechnol Adv* 25:294–306.
27. Keşan G, et al. (2016) Efficient light-harvesting using non-carbonyl carotenoids: Energy transfer dynamics in the VCP complex from Nannochloropsis oceanica. *Biochim Biophys Acta* 1857:370–379.
28. Carbonera D, et al. (2014) Photoprotective sites in the violaxanthin-chlorophyll a binding protein (VCP) from Nannochloropsis gaditana. *Biochim Biophys Acta* 1837:1235–1246.
29. Vieler A, et al. (2012) Genome, functional gene annotation, and nuclear transformation of the heterokont oleaginous alga Nannochloropsis oceanica CCMP1779. *PLoS Genet* 8:e1003064.
30. Li X-P, et al. (2000) A pigment-binding protein essential for regulation of photosynthetic light harvesting. *Nature* 403:391–395.
31. Umetani I, Kunugi M, Yokono M, Takabayashi A, Tanaka A (2018) Evidence of the supercomplex organization of photosystem II and light-harvesting complexes in Nannochloropsis granulata. *Photosynth Res* 136:49–61.
32. Litvín R, Bína D, Herbstová M, Gardian Z (2016) Architecture of the light-harvesting apparatus of the eustigmatophyte alga Nannochloropsis oceanica. *Photosynth Res* 130:137–150.
33. Peers G, et al. (2009) An ancient light-harvesting protein is critical for the regulation of algal photosynthesis. *Nature* 462:518–521.
34. Alboresi A, Gerotto C, Giacometti GM, Bassi R, Morosinotto T (2010) Physcomitrella patens mutants affected on heat dissipation clarify the evolution of photoprotection mechanisms upon land colonization. *Proc Natl Acad Sci USA* 107:11128–11133.
35. Bailleul B, et al. (2010) An atypical member of the light-harvesting complex stress-related protein family modulates diatom responses to light. *Proc Natl Acad Sci USA* 107:18214–18219.
36. Demmig-Adams B, Garab G, Adams WW, III, Govindjee (2014) *Non-Photochemical Quenching and Energy Dissipation in Plants, Algae and Cyanobacteria* (Springer, Dordrecht, The Netherlands).
37. Young AJ, Frank HA (1996) Energy transfer reactions involving carotenoids: Quenching of chlorophyll fluorescence. *J Photochem Photobiol B* 36:3–15.
38. van Amerongen H, van Grondelle R (2001) Understanding the energy transfer function of LHCII, the major light-harvesting complex of green plants. *J Phys Chem B* 105:604–617.
39. Kloz M, et al. (2011) Carotenoid photoprotection in artificial photosynthetic antennas. *J Am Chem Soc* 133:7007–7015.
40. Ma Y-Z, Holt NE, Li X-P, Niyogi KK, Fleming GR (2003) Evidence for direct carotenoid involvement in the regulation of photosynthetic light harvesting. *Proc Natl Acad Sci USA* 100:4377–4382.
41. Liao P-N, Holleboom C-P, Wilk L, Kühlbrandt W, Walla PJ (2010) Correlation of Car S(1) → Chl with Chl → Car S(1) energy transfer supports the excitonic model in quenched light harvesting complex II. *J Phys Chem B* 114:15650–15655.
42. Holleboom C-P, Walla PJ (2014) The back and forth of energy transfer between carotenoids and chlorophylls and its role in the regulation of light harvesting. *Photosynth Res* 119:215–221.
43. Bode S, et al. (2009) On the regulation of photosynthesis by excitonic interactions between carotenoids and chlorophylls. *Proc Natl Acad Sci USA* 106:12311–12316.
44. Dreuw A, Fleming GR, Head-Gordon M (2003) Charge-transfer state as a possible signature of a zeaxanthin–chlorophyll dimer in the non-photochemical quenching process in green plants. *J Phys Chem B* 107:6500–6503.
45. Holt NE, et al. (2005) Carotenoid cation formation and the regulation of photosynthetic light harvesting. *Science* 307:433–436.
46. Billsten HH, et al. (2005) Excited-state processes in the carotenoid zeaxanthin after excess energy excitation. *J Phys Chem A* 109:6852–6859.
47. Polívka T, Sundström V (2004) Ultrafast dynamics of carotenoid excited states-from solution to natural and artificial systems. *Chem Rev* 104:2021–2071.
48. Bailleul B, Cardol P, Breyton C, Finazzi G (2010) Electrochromism: A useful probe to study algal photosynthesis. *Photosynth Res* 106:179–189.
49. Cao S, et al. (2013) A transthylakoid proton gradient and inhibitors induce a non-photochemical fluorescence quenching in unicellular algae Nannochloropsis sp. *FEBS Lett* 587:1310–1315.
50. Kondo T, et al. (2017) Single-molecule spectroscopy of LHCSR1 protein dynamics identifies two distinct states responsible for multi-timescale photosynthetic photoprotection. *Nat Chem* 9:772–778.
51. Bennett DIG, Fleming GR, Amarnath K (2018) Energy-dependent quenching adjusts the excitation diffusion length to regulate photosynthetic light harvesting. *Proc Natl Acad Sci USA* 115:E9523–E9531.
52. Porra RJ, Thompson WA, Kriedemann PE (1989) Determination of accurate extinction coefficients and simultaneous equations for assaying chlorophylls a and b extracted with four different solvents: Verification of the concentration of chlorophyll standards by atomic absorption spectroscopy. *Biochim Biophys Acta* 975:384–394.
53. Leuenberger M, et al. (2017) Dissecting and modeling zeaxanthin- and lutein-dependent nonphotochemical quenching in *Arabidopsis thaliana*. *Proc Natl Acad Sci USA* 114:E7009–E7017.
54. Sylak-Glassman EJ, et al. (2014) Distinct roles of the photosystem II protein PsbS and zeaxanthin in the regulation of light harvesting in plants revealed by fluorescence lifetime snapshots. *Proc Natl Acad Sci USA* 111:17498–17503.
55. Müller-Moulé P, Conklin PL, Niyogi KK (2002) Ascorbate deficiency can limit violaxanthin de-epoxidase activity in vivo. *Plant Physiol* 128:970–977.